Bubbles Growing in Supersaturated Solutions at Reduced Gravity

N. Divinis
Dept. of Chemistry, Aristotle University, Univ. Box 116, 541 24 Thessaloniki, Greece
and
Dept. of Mechanical and Industrial Engineering, University of Thessaly, Greece

T. D. Karapantsios and M. Kostoglou
Dept. of Chemistry, Division of Chemical Technology, Aristotle University, Univ. Box 116, 541 24 Thessaloniki, Greece

C. S. Panoutsos and V. Bontozoglou
Dept. of Mechanical and Industrial Engineering, University of Thessaly, Pedion Areos, 38 334 Volos, Greece

A. C. Michels, M. C. Sneep, R. De Bruijn, and H. Lotz
Van der Waals–Zeeman Instituut, Universiteit van Amsterdam, 1018 XE Amsterdam, The Netherlands

DOI 10.1002/aic.10240
Published online in Wiley InterScience (www.interscience.wiley.com).

This work investigates bubbles growing in a liquid saturated with a dissolved gas when its temperature is locally raised above its saturation value, yet below boiling. Local supersaturation is realized by giving heat pulses of variable power and duration to a miniature heater. The experiments are conducted in a low-gravity environment to decouple bubble growth from buoyancy effects. A diffusion model is formulated considering the spherical growth of an internally heated bubble inside a uniformly subcooled liquid. The simple case of an isothermal bubble growth is solved analytically and compared to measurements to gain some physical insight. Two distinct regions are identified in the measured bubble growth curves: the initial stages are satisfactorily described by a parabolic (diffusion) law, whereas the later stages are approximately linear. © 2004 American Institute of Chemical Engineers *AIChE J,* 50: 2369–2382, 2004
Keywords: bubble growth, low gravity, diffusion, heat transfer, mass transfer

Introduction

Bubble generation and growth in liquids plays a key role in diverse fields of technology such as polymer (foam molding) and glass processing, flotation separations, pumps, and hydraulic power recovery systems (for example, Arefmanesh et al., 1992; Clift et al., 1978; Payvar, 1987; Yoo and Han, 1982). It also plays an important role in human physiology, such as blood oxygenation, bubbles growing in the tissue of airplane passengers, astronauts, and divers during decompression (for example, Foster et al., 2000; Kislyakov and Kopyltsov, 1988; Srinivasan et al., 2000; Van Liew et al., 1995). In addition, it is of critical value in studying physical phenomena such as cavitation, nucleation, and boiling (for example, Arefmanesh et al., 1991; Lee and Merte, 1996a,b; Plesset and Sadhal, 1982; Straub, 2000).

A large body of literature exists on the subject of bubble growth. The line separating bubble growth arising from over-

Correspondence concerning this article should be addressed to T. D. Karapantsios at karapant@chem.auth.gr.

saturation or chemical reaction from boiling is not clear because all these phenomena share common principles. In general, bubble growth is a complex process involving momentum, mass and heat transfer between an expanding bubble and the surrounding liquid.

Many of the earlier studies tried to predict scaling relationships of the form $R \sim t^{\alpha}$, where R is the bubble radius and t denotes the time period of growth. A classic theoretical account was communicated by Scriven (1959), who found that a simple parabolic law ($\alpha = 0.5$) describes bubble growth in an infinite liquid of constant supersaturation. In addition to molecular diffusion, his analysis takes into account the radial convective movement of the expanding gas–liquid interface, which results in a faster growth than expected for diffusion alone. Although originally meant to describe *nucleate boiling*, Scriven's solution has a general validity. For boiling of pentane Strenge et al. (1961) reported exponent values in the range $0.312 < \alpha < 0.512$, whereas in a study of nucleate boiling of water, Saddy and Jameson (1971) proposed that α is close to 0.75. Recently, Picker and Straub (2000) performed boiling experiments in microgravity conditions where vapor bubbles grew as the result of heat pulses inside an overall supersaturated liquid. These authors achieved the best fit to their data by taking $\alpha = 0.43$ that, given the experimental uncertainty, was considered adequately close to the parabolic predictions of Scriven. The diversity in the reported values of α for nucleation boiling reflects both difficulties in performing well-controlled experiments and also possible contributions from several rate-controlling mechanisms such as surface tension, viscosity, and inertia. The effects of these mechanisms were shown by Birkhoff et al. (1958) to be negligible, provided that the initial bubble size is not extremely small. On this account, Rosner and Epstein (1972) calculated deviations from the parabolic law for small bubbles (in a submicroscopic scale) attributed to finite interfacial kinetics and capillarity effects.

Studying bubble growth in a *solution supersaturated* with a dissolved gas, Buehl and Westwater (1966) obtained a value of α equal to 0.5. Bisperink and Prins (1994) and Barker et al. (2002) performed decompression experiments to study the growth of single bubbles in carbonated liquids and also found that a parabolic law fits their data nicely. In experiments where water was uniformly superheated (and not decompressed), Jones et al. (1999a) reported once more a parabolic growth of CO_2 bubbles, all the way from bubble inception to final detachment. In summary, there exists enough evidence in the literature that a parabolic law can adequately describe the isothermal bubble development ascribed to mass diffusion from a homogeneously supersaturated liquid.

At the other end of the line, there is a vast literature devoted to vapor bubbles growing because of *boiling over heated solid surfaces* (Dhir, 1998). The situation is now more complex because the bubble shape changes continuously during the growth process and superheated liquid is restricted to only a thin a region around the bubble (Mikic et al., 1970). Among these studies special reference must be made to Lee and Merte (1996a,b) and Straub and coworkers (1992, 1994, 2000), who performed meticulous pool boiling experiments in microgravity conditions to discard natural convection effects and avoid bubble distortion and departure from the heater. Apart from the experiments, Lee and Merte made decisive improvements in the theoretical models for both spherical growth in a uniformly superheated unbounded liquid and hemispherical growth in a nonuniform liquid temperature field such as that arising from a heated flat surface.

Surveying previous work as outlined above reveals that a full understanding of the mechanisms that govern bubble growth has not yet been reached. Serious work is still under way to achieve this goal by incorporating either more complex mathematical analyses or more elaborate experiments (for example, Robinson and Judd, 2001; Shaw and Pantoya, 2000).

In the past, diffusion induced bubble growth of a dissolved gas was triggered either by a homogeneous reduction in pressure or by a global increase in the bulk temperature of a saturated solution. These efforts were usually undertaken having in mind the mechanisms of nucleation rather than bubble growth (for example, Jones et al., 1999b). For this reason, most experiments were conducted at low temperatures where the effect of the liquid vapor pressure is insignificant. Apart from that, both experimental approaches provided data under isobaric and isothermal conditions where only concentration—and not thermal—gradients exist between the bubble and the liquid. In real applications, though, such ideal conditions are unlikely to occur and the simultaneous presence of temperature gradients is inevitable. Such thermal inhomogeneity can be produced in experiments where supersaturation is created at only a small confined region of a large pool of liquid by using a small local heater. Such experiments—although very interesting from both a fundamental and an applied perspective—when performed under terrestrial conditions are complicated to interpret because of the prevailing buoyancy effects, and have thus attracted no attention in the literature. A microgravity environment would skip these annoying effects and would further permit the investigation of considerably large bubbles, where not only the capacity of the diagnostics is better but also heat and mass transfer clearly dominate the desorption process.

The purpose of the present work is to study bubble growth of a dissolved gas in a solution due to local supersaturation. In the next sections the microgravity relevance in studying bubble growth is outlined first and then the basic equations underlying the associated phenomena are derived. In a first attempt to describe the complicated bubble dynamics, a similarity solution of the model equations is proposed based on the assumption of a constant bubble temperature. The main experimental information involves measurements of bubble radius vs. time under various conditions. These experiments were conducted during the low-gravity period achieved in the parabolic free-fall trajectory of an aircraft during two of ESA's (European Space Agency) parabolic flight campaigns. To our knowledge this is the first time that mass diffusion induced bubble growth experiments are performed in weightlessness. Finally, the obtained bubble growth data are contrasted against theoretical predictions in an effort to interpret the observed phenomena.

Microgravity Relevance

The influence of the level of gravity on the bubble shape is given by the balance between hydrostatic and capillary forces, expressed by the Bond number, $\mathrm{Bo} = (\rho_L - \rho_G)gD^2/\sigma$. The smaller the Bond number, the more spherical the bubble. Note that a perfect sphere is the case only when $\mathrm{Bo} = 0$, that is, when either g or $(\rho_L - \rho_G)$ equals zero. On earth, for gravitational distortion to be less than 1% of the total strain we must

satisfy the inequality $(\rho_L - \rho_G)gD^2/[(\rho_L - \rho_G)gD^2 + \sigma] < 0.01$. For water this condition leads to $D < \sim 0.25$ mm but for most organic liquids D must be less than 1/3 of this value. The size of these bubbles is quite small to study with conventional optical systems. This is not a problem of magnification. The problem stems from the very limited depth of field in such high magnifications, which not only makes the focusing of the bubble exceedingly cumbersome but also does not allow for a sharp image when monitoring the different sizes of a growing bubble.

Under low-gravity conditions individual bubbles remain attached to the heater surface for longer times and therefore grow to excessively large sizes without departing from the heater surface. It has been repeatedly observed (for example, Straub et al., 1990, 1992) that bubbles at microgravity will remain about 10 times longer at the heater surface and grow to a diameter 3 to 4 times larger than in 1 g before they depart. Eventual bubble departure occurs mainly because of Marangoni convection or g-jitters.

Gravity can create significant mass flow in the bulk of the liquid even under small temperature gradients. This is attributed to natural convection caused by density stratification. Such phenomena show up when the Grashof number ($Gr = g\beta\rho^2\Delta T D^3/\mu^2$) is much larger than unity, that is, when both bubble size and ΔT are large. In addition, significant liquid agitation may be produced by departing prior bubbles. On the contrary, at $g \approx 0$ such concerns are irrelevant.

Theory

The particular problem studied herein involves bubble growth on the surface of a solid heater. However, the characteristics of the experiment are such that permit a crude first approximation based on an isotropically growing spherical bubble. More specifically, the surface of the thermistor is coated with a thin glass layer and, because glass is highly wettable, the advancing contact angle between the thermistor and the liquid for a slow growing bubble is appreciably small. This is more so with apolar (organic) low-energy liquids, which tend to have an approximately zero contact angle with a solid surface. Besides, there is prior theoretical and experimental work (for example, Buehl and Westwater, 1996; Glas and Westwater, 1964) supporting that the effect of contact angle on bubble growth rates is very small. Therefore at all times the bubble is assumed to attain a spherical shape with a minimal contact with the solid. In addition, the heater has a highly curved (roughly spherical) surface and, as a consequence, a slight displacement of the contact line between the bubble and the heater (while maintaining constant contact angle) would require a large volume change of the bubble. This means that in the present case the small contact area between the bubble and the heater changes only slightly as the bubble grows at just a reasonable size. Besides, after some time the size of the bubble becomes larger than the size of the heater.

The above characteristics, supplemented by the elimination of gravity, permit as a first approximation the consideration of a perfectly spherical bubble and the substitution of the heated surface by a heat source in the center of the bubble. Evidently, this assumption is in error at the very first instants of growth where a bubble cup appears instead, but this work is not concerned with this time regime (typically for $t < 10$ ms; Straub, 2000). Bubble sphericity leads to a major simplification of the mathematical model, which becomes one-dimensional (1-D). Campos and Lage (2000) used a similar assumption in simulating the formation of superheated bubbles at an orifice. In their 1-D bubble growth model, they substituted the orifice with a gas source in the center of the sphere.

The gas bubble growth problem is associated with various timescales. These are the mass diffusion and heat conduction timescales in gas and liquid phase in pairs. The significance of each timescale can be assessed by comparison with the bubble growth timescale. Whereas the transport timescales in the liquid are comparable to that of bubble growth, transport phenomena in the gas phase are much faster. This means that the concentration and temperature in the bubble can be taken in our model as uniform. In addition, compressibility effects may be safely neglected for the relatively small bubble growth velocities encountered in the present experiments and the pressure inside the bubble can be assumed as uniform.

A description of the growth of a bubble requires the coupling of the equations for continuity, motion, conservation of the diffusing species, and heat transfer. The equation of motion of the bubble (Rayleigh–Plesset equation) under the present conditions degenerates to

$$P_v + P_g = P_\infty \tag{1}$$

where P_∞ is the external (ambient) pressure, P_g is the partial pressure of CO_2, and P_v is the vapor pressure of the liquid. The terms that contain time derivatives of the bubble radius R, in the Rayleigh–Plesset equation, can be neglected because of the slow growth of the bubble. These terms are important in boiling applications where typical growth rates are of the order of mm/μs. The contribution of surface tension (Laplace pressure) to bubble evolution has been studied in detail by Cable and Frade (1988). They found that for bubbles with radius 20 times larger than the critical radius, the effect of surface tension is negligible. In the present case the critical radius is of the order of 1 μm so surface tension can be safely ignored in Eq. 1.

The equation of continuity in the liquid phase requires that the (radial) liquid velocity u has the following form (assuming the density of the bubble is negligible with respect to the density of the liquid),

$$u = \frac{R^2}{r^2}\dot{R} \tag{2}$$

where the overdot denotes the time derivative.

The energy conservation equation in the liquid phase is

$$\frac{\partial T}{\partial t} = K\left(\frac{\partial^2 T}{\partial r^2} + \frac{2}{r}\frac{\partial T}{\partial r}\right) - \dot{R}\,\frac{R^2}{r^2}\frac{\partial T}{\partial r} \tag{3}$$

where K is the thermal diffusivity of the liquid phase.

The solute mass conservation equation in the liquid phase is

$$\frac{\partial C}{\partial t} = D\left(\frac{\partial^2 C}{\partial r^2} + \frac{2}{r}\frac{\partial C}{\partial r}\right) - \dot{R}\,\frac{R^2}{r^2}\frac{\partial C}{\partial r} \tag{4}$$

where C is the concentration of CO_2 and D is the diffusivity of CO_2 in the liquid.

A mass balance of CO_2 on the bubble surface gives

$$\frac{d(\rho_g R^3)}{dt} = 3DR^2\left(\frac{\partial C}{\partial r}\right)_{r=R} \tag{5}$$

where ρ_g is the molar density of CO_2 in the gas phase.

The boundary conditions on the gas–liquid interface are the continuity of the temperature (the subscript B denotes the bubble)

$$T(R, t) = T_B(t) \tag{6}$$

and the equilibrium of CO_2 in the two phases (Henry's Law)

$$C(R, t) = C_{sat}(T_B) \tag{7}$$

where $C_{sat}(T_B)$ is the solubility of the gas for temperature T_B and total pressure P_∞ or equivalently for partial pressure P_g.

Finally, the temperature dependency of the water vapor pressure and the law of ideal gases for the CO_2 are needed to close the problem

$$P_v = P_{sat}(T_B) \tag{8}$$

$$\rho_g = \frac{P_g}{R_g T_B} \tag{9}$$

where R_g is the universal gas law constant.

The initial conditions of the problem are as follows.

Uniform Initial Temperature

$$T(r, 0) = T_0 \tag{10}$$

Uniform Concentration of Dissolved CO_2 in Equilibrium with the Gas Phase

$$C(r, 0) = C_0 = C_{sat}(T_0) \tag{11}$$

and

$$R = R_0 \tag{12}$$

The initial size of the bubble must be the critical size. However, this size is a function of the supersaturation, which for the present problem evolves with time so it is not known in which supersaturation the bubble will be formed. Nevertheless, an exact value for R_0 is of little significance because, as with the surface tension, very soon the bubble does not retain its initial size.

The boundary conditions far from the bubble are:

$$T(\infty, t) = T_0 \tag{13}$$

$$C(\infty, t) = C_0 \tag{14}$$

The global heat balance for the bubble is

$$\frac{W}{A} = \frac{V}{A}(\rho_g c_g + \rho_v c_v)\frac{dT_B}{dt} + P_\infty \frac{dR}{dt} + E_a \frac{d\rho_g V}{A dt} + L\frac{d\rho_v V}{A dt} - k\left(\frac{\partial T}{\partial r}\right)_{r=R} \tag{15}$$

where A and V are the surface area and the volume of the bubble, respectively; ρ_v is the vapor molar density in the bubble; c_g and c_v are the specific heat capacities of the CO_2 and vapor, respectively; L is the latent heat of liquid; E_a is the dissolution energy of CO_2 in the liquid; and k is the thermal conductivity of the liquid phase. All the above properties must be computed for a temperature equal to T_B. The left-hand side of Eq. 15 is the energy rate given to the bubble from the heater (spherical thermistor). On the right-hand side of the equation the first term is the rate of the sensible heat needed to raise the bubble temperature; the second term is the rate of the gas expansion work; the third and fourth terms are the rate of the energy consumed for the dissolution of CO_2 and evaporation of water, respectively; and the final term is the rate of heat transfer from the liquid to the bubble.

The above system of equations is by no means trivial to solve and studies of considerable effort have been reported in the literature. The main difficulty is the solution of the transient convection–diffusion Eqs. 3 and 4 with a moving boundary. Several approximate solutions have been developed based on the relative magnitude between convection and diffusion (Arefmanesh et al. 1992; Lee and Merte, 1996b; Plesset and Zwick, 1954; Rosner and Epstein, 1972).

A review of the approximate solutions of the complete bubble growth problem (either with gas diffusion or evaporation) is presented by Vrentas et al. (1983). These authors found that the above system of equations may possess a self-similar solution in the limit of large time. The essence of the self-similarity approach is that all terms in Eqs. 5 and 15 have the same time dependency. More specifically, the bubble radius increases proportionally to $t^{1/2}$. In the present case, the self-similarity may be destroyed by the term describing the rate of heat given to the system, W, which is an input function, and therefore has arbitrary time dependency. For the self-similarity to be retained, W should also increase proportionally to $t^{1/2}$ and then the resulting bubble temperature is constant. In other words, assuming a constant bubble temperature is equivalent to assuming that $W \propto t^{1/2}$. This simplified case is examined below.

The constant bubble temperature case [$T_B(t) \cong T_e$]

By use of a constant bubble temperature as input variable to the above equations one can determine independently the growth rate of the bubble and the required heat input rate because then the mass and heat transfer problems are decoupled. The following nondimensionalization is introduced

$$\tau = \frac{T - T_0}{T_0} \qquad \tau_e = \frac{T_e - T_0}{T_0}$$

$$c = \frac{C - C_0}{C_0} \qquad c_e = \frac{C_{sat}(T_e) - C_0}{C_0} \tag{16}$$

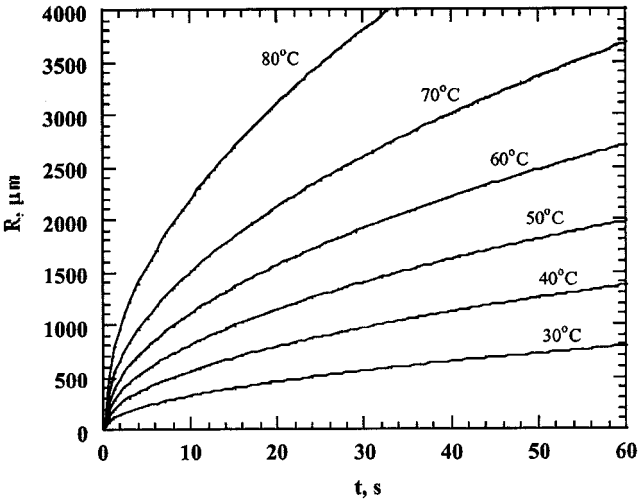

Figure 1. Theoretical predictions of bubble radius vs. time for several constant bubble temperatures.

The heat transfer equation takes the form

$$\frac{\partial \tau}{\partial t} = K\left(\frac{\partial^2 \tau}{\partial r^2} + \frac{2}{r}\frac{\partial \tau}{\partial r}\right) - \dot{R}\,\frac{R^2}{r^2}\frac{\partial \tau}{\partial r} \qquad \text{in } R < r < \infty \quad (17)$$

The initial/boundary conditions are

$$\tau(r, 0) = 0 \qquad \tau(R, t) = \tau_e \qquad \tau(\infty, t) = 0 \quad (18)$$

The mass transfer equation and the relevant conditions have exactly the same form but with c in place of τ and D in place of K.

The self-similarity solution of the above system proceeds as follows. Let us assume

$$s = \frac{r}{2\sqrt{Kt}} \quad (19a)$$

and

$$R = 2\beta\sqrt{Kt} \quad (19b)$$

The solutions of the above equations are

$$\tau = \tau_e \frac{I(s, \beta)}{I(\beta, \beta)} \qquad c = c_e \frac{I(\lambda s, \lambda\beta)}{I(\lambda\beta, \lambda\beta)} \quad (20)$$

where

$$\lambda = \sqrt{\frac{K}{D}} \quad (21a)$$

and

$$I(x, \beta) = \int_x^\infty \frac{1}{y^2} e^{-y^2 - 2\beta^3/y} dy \quad (21b)$$

Substitution in the interface condition (Eq. 5) leads to

$$\varphi(\beta\lambda) = \Psi \quad (22a)$$

where

$$\varphi(z) = I(z, z) 2z^3 e^{3z^2} \quad (22b)$$

and

$$\Psi = \left\{\frac{P_\infty - P_{sat}(T_e)}{[C_{sat}(T_e) - C_{sat}(T_0)]R_g T_e}\right\}^{-1} \quad (22c)$$

The energy input that is needed to achieve a constant bubble temperature can be shown after some algebra to be

$$W = 2\gamma\sqrt{Kt} \quad (23)$$

where

$$\gamma = 8\pi\beta^3\left[BK + k(T_e - T_0)\frac{1}{\varphi(\beta)}\right] \quad (24)$$

and

$$B = P_\infty + (\rho_g E_a + \rho_v L) \quad (25)$$

An asymptotic approximation of the above solution, which is particularly convenient for computations, is presented in the Appendix.

Figure 1 presents theoretical predictions of bubble radius vs. time for several constant bubble temperatures. Results are for the system CO_2 dissolved in water. Table 1 displays indicative values (at 25°C) of the thermophysical properties of all the liquids used in this study. Within a few seconds the bubble reaches a considerable size, which is largely dependent on temperature. The increasing contribution of the vapor pressure of water at higher temperatures is evident because it results in an excessively faster bubble growth as the temperature rises.

The self-similarity solution is obtained under the assumption

Table 1. Indicative Transport Properties at 25°C for the Three Liquids Used

Liquid	Solubility, C (gmol/cm^3)	Diffusion Coefficient, D (cm^2/s)	Boiling Temperature T_B (°C)
Water	3.49×10^{-5} [i,ii]	1.81×10^{-5} [iii,iv]	100[iv]
n-Heptane	2.56×10^{-4} [iv]	6.47×10^{-5} [iii,iv]	98.4[iv]
Glycerin–water 80–20%, w/w	N/A	6.96×10^{-7} [iii,iv]	Glycerin: 290[iv] Water: 100

[i]Lide and Frederikse (1996–1997).
[ii]Perry and Chilton (1973).
[iii]Reid et al. (1986).
[iv]http://factrio.jst.go.jp/cgi-bin/al_m_login.csh.

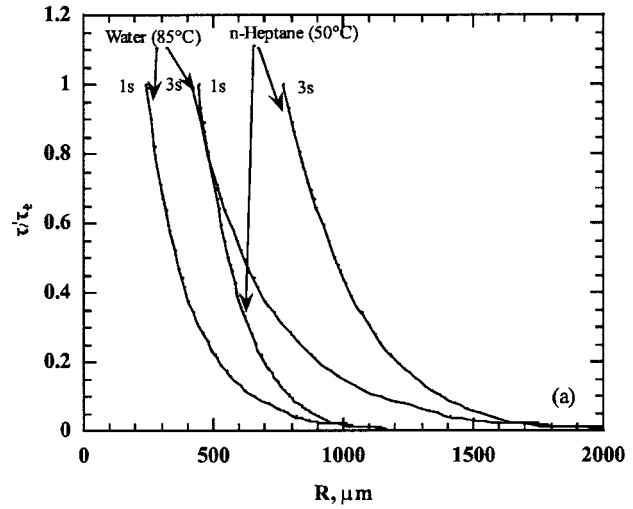

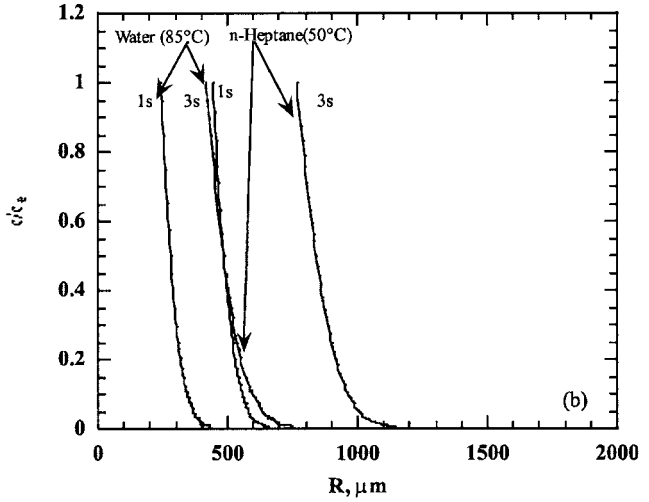

Figure 2. Predicted (a) temperature and (b) concentration boundary layers around a bubble at two instants (1 and 3 s) of its growth.

of a constant thermal conductivity and diffusivity in the liquid with values corresponding to the constant bubble temperature. This assumption is not generally valid because of the existence of temperature and concentration gradients around the bubble. For highly diluted solutions the conductivity and diffusivity dependencies on concentration are small. Also, the dependency of conductivity on temperature, in the range of values appearing in the present problem, is small and can be ignored. On the other hand, the temperature dependency of diffusivity is appreciable and cannot be ignored as easily. Figure 2 displays the estimated temperature and concentration boundary layers extending outside a bubble at two different instants (1 and 3 s) of its growth. Predictions are for water and *n*-heptane and for bubble temperatures like those typically measured for the two liquids in this work. For both liquids the concentration boundary layer is substantially smaller than the temperature boundary layer, which is more prominent for water. The parameter that expresses the relative size of the two boundary layers is λ (Eq. 21a), which is 4.9 (at 85°C) for water and 3.2 (at 50°C) for heptane. This means that, at least during the early stages of growth, mass diffusion occurs in a region near the bubble surface where the temperature varies in just a narrow range. So, to a first-order approximation, the diffusivity can be assumed initially constant and equal to its value for temperature T_B. In principle, however, a complete solution must also take into account the temporal and spatial variability of conductivity and diffusivity with temperature.

Experimental

Setup

The core of the equipment is a thermostat unit into which an exchangeable sample cell unit is inserted (Figure 3). The thermostat is a CPF-2 type, flown in prior shuttle missions (de-Bruijn et al., 1997). The thermostat operates under the gradient reduction principle and is capable of temperature ramps of 0.02–500 μK/s at spatial gradients of <10 μK/mm. The low thermal resistivity of the structure and the use of Peltier elements enable fast changes of the temperature set point of the thermostat and thus substantially reduce the time for thermal adjustments. The thermostat can provide precise temperature stability in the order of ± 0.005°C. In addition, the thermostat is also equipped with optical and electronic interfaces that enable the stimulation and observation of the test fluid.

A sample cell unit is essentially a sealed tube, the lower part of which is made of special spectrometer glass cuvette with an internal diameter of 1.5 cm. The cells are specially designed to maintain their measuring chamber (glass cuvette) completely full with liquid in all times so as to prevent free float of the liquid in microgravity. The liquid volume in the cell is about 22 cm^3. The pressure inside the cells is kept at ambient values by means of an elastic membrane sealing a port of the cell. Two types of heaters are accommodated inside the test cells, placed apart by 5.5 cm in the longitudinal direction: a small axisymmetrical NTC thermistor (Thermometrics, Inc., Edison, NJ; $r_{th} = 0.125$ mm, nominal), to serve as a point spherical heater; and a flat platinum resistance layer (3×7 mm, about 1 mm thick) deposited on a special nonconducting support, to serve as a flat surface heater. Here, results only from the former will be presented.

The bubbles growing on the spherical heater are illuminated by RGB light-emitting diodes (LEDs) and recorded by a CCD color camera with $1k \times 1k$ pixels, 24-bit resolution RGB, and an acquisition rate of 25 frames/s. Constant-power ($\pm 2\%$) heating pulses are applied to the heating thermistor through a special circuitry. Registering the voltage drop across the heater allows the delivered power and temperature of the heater to be calculated. A thermistor (same size as the heating thermistor) measures the bulk liquid temperature at a distance 2.5 mm from the heater surface with a maximum uncertainty of ± 0.05°C. The thermal performance of the equipment is controlled and supervised by custom-made software.

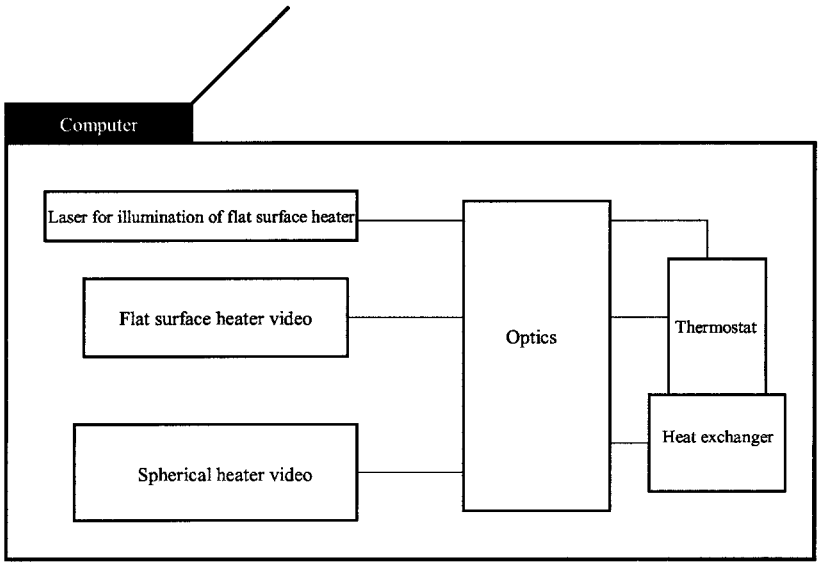

SIDE VIEW

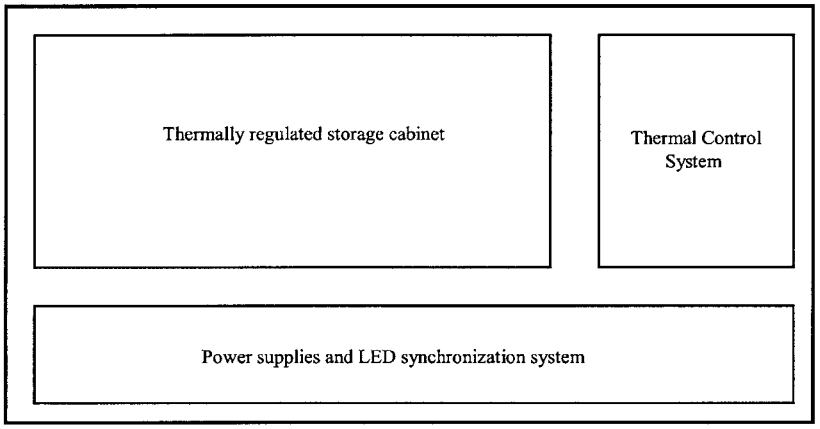

TOP VIEW

Figure 3. Experimental apparatus.

Water and *n*-heptane are the basic test liquids examined in this study. A few runs are also performed with a mixture of glycerin–water (80–20% w/w). All liquids are saturated with CO_2, a gas chosen mainly because of its practical significance and its large solubility in liquids, which easily generates the phenomena we wish to investigate.

Procedures

The experiments were performed during two of ESA's Parabolic Flight Campaigns. Meaningful quantitative information was gathered chiefly at the second campaign because the first one was devoted in precursory experiments aiming to identify the useful range of experimental parameters. On the whole, 48 runs were successfully performed with the small spherical heater, and the rest with the plate heater. Each parabolic trajectory provides a sequence of normal–high–low–high–normal gravity levels. The gravity level during the low-gravity phase fluctuates randomly within $\pm 5 \times 10^{-2}$ g, whereas during the high-gravity phase the level reaches a peak value of about 1.8 g. The low-gravity period is slightly different among parabolas but on the average is around 20 s.

The saturation of the test liquids with CO_2 was conducted on the ground just before the flight. This was realized by bubbling the liquids with the gas at 32°C for about 60 min. This time lapse was chosen based on wet analysis of water samples exposed to CO_2 bubbling for varying time intervals (Bontozo-

glou and Karabelas, 1995). Next, the saturated liquids were used to fill 10 sample cell units. A thermally regulated storage cabinet, part of the flight apparatus, was used to maintain the test cells hermetically closed at a temperature 2°C below the saturation temperature.

A brief outline of the experimental scenario is as follows. An exchangeable test cell is inserted in the thermostat and is left to equilibrate at a temperature a few tenths of a degree below the liquid's saturation temperature. Then the temperature of the liquid is raised locally by energizing the heater at a preset power level and duration. This is done about 5 s after the onset of low gravity to ensure that the experiment would start at low-gravity conditions. A short time delay is necessary to create local superheat and therefore cause nucleation, after which a bubble forms and grows on the thermistor's surface. After five consecutive parabolas the test cell is exchanged with a new one.

Different power levels are delivered to the small spherical heater in the range 12 to 102 mW. Assuming that the heater is roughly spherical, these power levels correspond to heat fluxes between 0.47×10^5 and 3.6×10^5 W/m^2 and temperatures of the thermistor between 37°C and 108°C. The duration of heat pulses is varied between 10 and 30 s.

Image processing of video frames to determine the bubble diameter is performed by a code written in MATLAB (The MathWorks, Natick, MA). The bubble is seen as a bright RGB image against a darker background. The three illumination colors give marginally different sizes because of their lateral chromatic aberration (different refractive index) and also because of their slightly different latitude (angle of incidence) with respect to the bubble's equator. The disparity among colors regarding bubble size is at most $\pm 2\%$. As a convention, the maximum size is always taken as the real size of the bubble regardless of the color producing it. This is done on the premise that, under identical experimental conditions, the overall uncertainty in the measured bubble radius is nonetheless $\pm 3\%$. The known speed of the camera allows determination of bubble radius as a function of time.

Results and Discussion

Visual observations

Nucleation of single bubbles occurs exclusively at a specific site on each thermistor. This site is independent from power, temperature, or test liquid. Such a preferential nucleation is usually attributed to vapor/gas trapped in submicroscopic imperfections, such as cavities or scratches, on the thermistors' surface (Jones et al. 1999b).

After the initial thermalization of the heater some time is needed for nucleation to occur. The nucleation delay time varies from one test liquid to another but also among runs with the same liquid. In *n*-heptane, nucleation is almost instantaneous; in water it usually occurs in less than 1 s, although there are a few runs where it took several seconds (up to 7). Finally, in glycerin/water mixtures nucleation is also a matter of 1 or 2 s. There is no clear relationship between nucleation time and power level or heating thermistor. An arbitrary fluctuation in nucleation delay time has been repeatedly reported in the past and was attributed to inevitable impurities and uncontrollable minor nonuniform superheats (for example, Lee and Merte, 1996b).

For all test fluids, bubble expansion is fast at the beginning and slows down drastically at later times. Bubbles grow faster and larger in *n*-heptane than in water, whereas in glycerin/water mixtures they grow even slower and smaller. The shape of the bubbles is spherical nearly from the very beginning of their growth and for all liquids. Even the smaller bubbles encountered in glycerin/water mixtures have a bubble-cup shape only at times below about 40 ms; the spherical shape is attained for the rest of the growth process.

Smaller bubbles are, in general, stiff and robust, whereas larger bubbles are sensitive to vibrations and floppy. For *n*-heptane, the high-gravity phase after the low-gravity one is always capable of removing any bubbles adhering to the surface of the thermistor. These bubbles almost always leave the field of view of our camera, probably because of g-jitters or Marangoni convection and either remain floating in the bulk of the liquid or reach and adhere to the walls of the test cell. However, this does not happen all the time with water and it *never* happens with glycerin/water mixtures, where bubbles, once created on the thermistor, cannot be removed because of the high viscosity of the fluid. Remaining bubbles pose a serious constraint for conducting multiple runs with the same test cell.

Thermal data

The thermal condition of the bulk liquid during heat pulses is of primary concern. On the average, the temperature measured by the thermistor located 2.5 mm in the longitudinal direction away from the heater increases by less than 0.2°C during heat pulses. So, the bulk liquid is effectively not influenced by the local heating.

Because of the low heat capacity of the heating thermistor, the thermistor reaches its final temperature in less than 1 s. During the initial stages of bubble growth, the thermistor's readings decay rapidly because an increasing amount of heat (proportional to the bubble's surface area) is progressively claimed from the thermistor that acts as a low-heat–capacity energy reservoir. Figure 4a displays such a typical temperature profile during a heat pulse given in water, where two limiting temperature values (T_{max}, T_{min}) are noted. The [x, x, x] format in the legend stands for [run no., power, T_{max}/T_{min}].

The rate of the initial rapid temperature decay in Figure 4a is inversely proportional to the delivered power. Figure 4b shows the relation between the delivered power and the two limiting temperatures for the runs where just a single bubble grows at a time. An approximately linear increasing trend is observed between power and temperature, demonstrating that the thermal condition of the thermistor is strongly associated with power. Some scatter is attributed to the slightly different electrical characteristics of the different thermistors. It is noteworthy that *different* power levels (and temperatures) generate *single* bubbles in the two liquids; the higher values are used with water and the lower ones with *n*-heptane. Low powers do not produce any bubbles in water, whereas high powers produce multiple simultaneous bubbles in heptane.

An ascending temperature spike is observed when a (large) bubble departs from the thermistor's surface; the temperature drops again as soon as a new bubble arises in its place (see in next section). These spikes are more pronounced in *n*-heptane ($\sim$10°C). Similar spikes were observed during new bubble

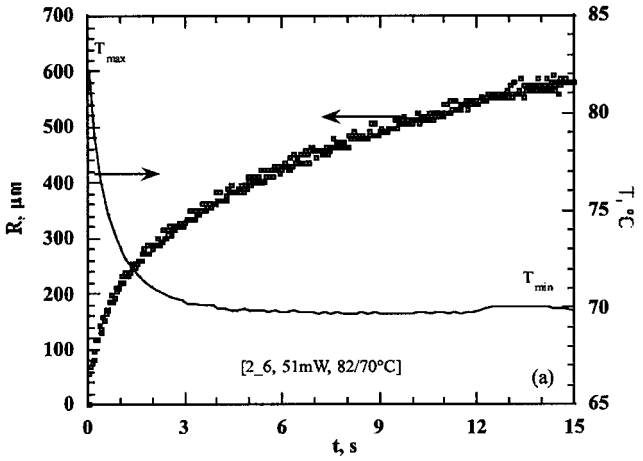

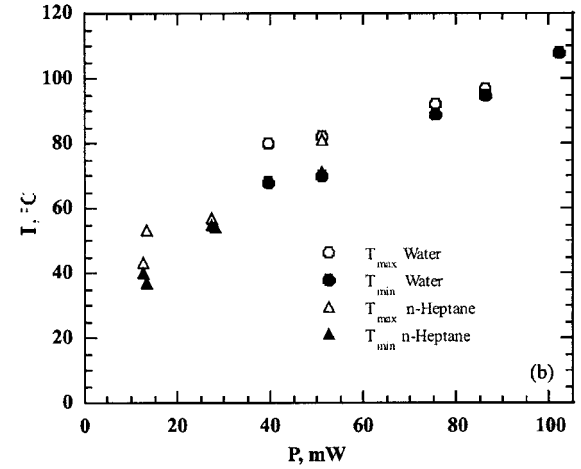

Figure 4. (a) Bubble growth data and the associated temperature decay of the heating thermistor during a heat pulse; (b) maximum and minimum thermistor temperatures during heat pulses vs. the power delivered.

generation in boiling experiments and found to substantially enhance heat transfer (Chen and Chung, 2002).

Bubble growth data

The effect of the different gravity levels (during a parabola) on growing bubbles is demonstrated in Figure 5. As displayed, the low-gravity period (~0 g) is followed by a transition period (~0 → 1.6 g) toward a high-gravity period (~1.6 → 1.8 → 1.6 g), which is subsequently succeeded by a transition period (~1.6 → 1 g) toward normal gravity (~1 g). It must be recalled that heat pulses start (t = 0 s) 5 s after the onset of a parabola. Two runs (A and B) are included in this graph, both conducted with water and the same test cell but at different power levels. Two bubbles are produced during heat pulses (A1 + A2 and B1 + B2). The two bubbles do not coexist but the second one emerges (at the same site) after the first one has departed from the thermistor.

As soon as bubbles A1 and B1 enter the first transition period they start to deviate from their prior course of growth and eventually leave the thermistor. Right after their detachment, bubbles A2 and B2 form and develop until the end of the heat pulses. The last part of the A2 and B2 curves occurs inside the high-gravity period. Comparison of the A1, B1 with the A2, B2 curves gives the impression that the bubbles grow differently at different gravity levels. However, this is purely an experimental artifact because the bubbles are no longer spherical and image analysis is fooled. The moment the heat pulses terminate, the bubbles immediately stop expanding, implying that thermal inertia effects ascribed to the heat capacity of the thermistor are negligible.

The relatively poor quality of low gravity conditions achieved in parabolic flights create disturbances in measurements because bubbles become more sensitive to external vibrations as they grow larger. A manifestation of the effect of vibrations is the progressively increasing high-frequency scatter in the measured growth curves as the bubble size increases. Minor temperature differences around the bubble might also create disturbances, attributed to Marangoni convection, but at much lower frequencies.

Figure 6 presents a representative run in *n*-heptane where three bubbles grow in a row; that is, at every instant there is just one bubble growing on the thermistor's surface. All bubbles are generated at exactly the same nucleation site. The temperature profile is also shown for comparison. As can be seen, at a radius around 800 μm the bubbles become sensitive to circumstantial external vibrations. Excluding the noise slightly before their detachment, the three bubble growth histories practically coincide if superimposed with no delay (nucleation) time between bubbles. These observations are contrary to what

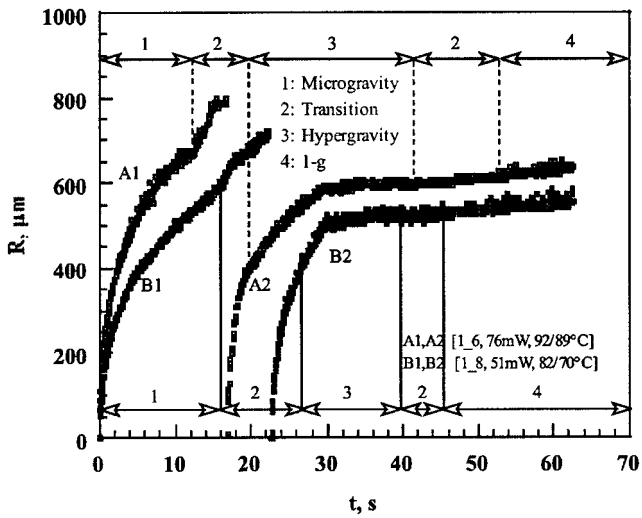

Figure 5. Effect of the different gravity levels during a parabola to growing bubbles.

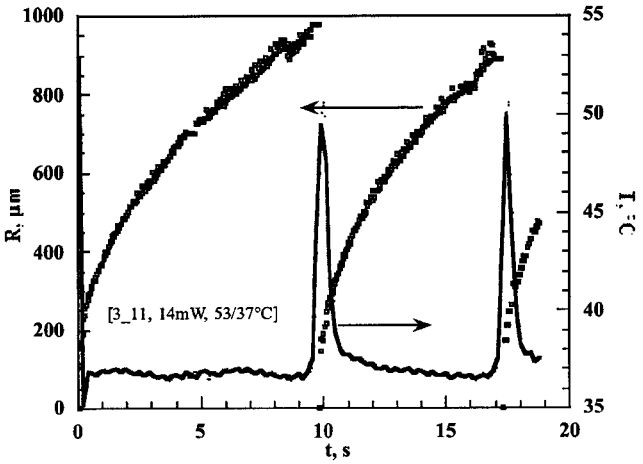

Figure 6. Three bubbles growing one after the other in *n*-heptane.

Bubble growth and temperature data.

is measured with bubbles growing in carbonated water (Buehl and Westwater, 1966; Jones et al., 1998), where every successive bubble had a longer nucleation lapse time and a slower growth rate than those of its predecessor, indicating a localized solute depletion at the region of the nucleation site. In general, when working with *n*-heptane and the power is high enough, two or more bubbles have the time to grow sequentially (and detach) within the same low-gravity period.

Figure 7 compares (single) bubble growth data for the three test fluids. The visual observations presented before are in accordance with measurements. Indeed, the fastest and largest growth is observed in *n*-heptane, whereas the slowest and smallest growth is seen in glycerin/water mixtures. If one further takes into account the power levels and temperatures of the thermistors, it is evident that the rate of growth and ultimate size of bubbles depend more on the physical properties of the fluids than on the delivered power and temperature.

What is perhaps more interesting in Figure 7 is the particular shape of the growth curves, which is common among all the curves of this work. At the beginning there is a parabolic growth region ($R \sim t^{0.5}$), which gradually levels off to an approximately linear region. This behavior is distinctly different from what has been observed in previous diffusion-induced growth experiments where the parabolic law was found to describe the bubble growth all the way from inception to final detachment (for example, Jones et al., 1999a). It must be stressed, however, that in those experiments the bubbles were growing in uniformly and not locally supersaturated liquids.

When working with the same test fluid, the delivered power and the temperature of the thermistor play a dominant role on the growth rate of single bubbles. This is shown in Figure 8a, which displays growth data for water (only five runs are included for clarity). Just the first 12 s of these runs are presented to avoid the excessive scattering resulting from vibrations. As the power and temperature of the thermistor increase, the rate of bubble growth increases. However, this trend is not sustained beyond a certain power and temperature level, after which any further increase has only a slight effect on growth (curves D and E). This upper limit is found for water to be around 90°C.

The solid lines in the graph represent self-similarity solutions of the model equations obtained for the measured initial temperatures (T_{max}) of the thermistors. Runs A and B agree quite well with the predictions of the model in the first 1–2 s. This time regime has been also found in nucleate boiling to be adequately described by a constant temperature parabolic law (for example, Lee and Merte, 1996a). Noticeably, for higher initial thermistor temperatures, the agreement between predictions and measurements is restricted to gradually shorter times. The model fails completely to describe runs D and E. In these two runs, the applied powers are the highest of all and yield a thermistor temperature of 97 and 108°C, respectively. No sign of boiling is observed on the thermistor's surface in the latter run. Using these values as input, the model severely overpredicts the bubble data, as shown in Figure 8a.

Runs with different power levels in heptane are compared in Figure 8b. To display exclusively single-bubble data and also discard disturbances in the signal, only the first 3 s of growth are presented. As above, solid lines represent solutions of the model equations based on the initially measured temperatures (T_{max}) of the thermistors. It is apparent that as the initial temperature increases the isothermal diffusion model progressively fails to describe the growth. As in water, it seems that also in *n*-heptane there exists an upper temperature limit beyond which the growth rate is virtually constant. This temperature seems to be not far from 55°C.

Figure 8c displays one of the few single-bubble runs that were possible to obtain with the glycerin/water solution. It must be recalled that this is mainly because bubbles once created do not detach from the thermistor because of the high viscosity of the solution. The growth curve exhibits the same general features with those measured in water and *n*-heptane. No theoretical predictions are drawn in the graph mainly because the physical properties of the solution could not be reliably obtained from the literature (Table 1 presents only indicative values estimated from weighted averages for water and glycerin). What is noteworthy when a single bubble grows in the glycerin/water solution is that the growth always ceases (a plateau) before the end of the heat pulse and when the bubble

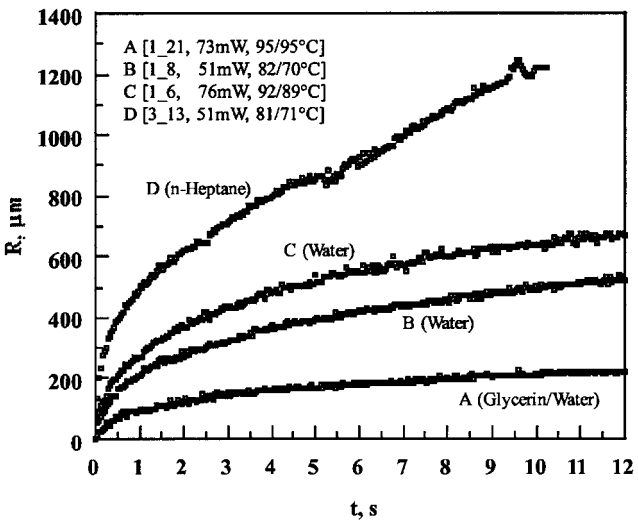

Figure 7. Single bubble growth data for the three test fluids.

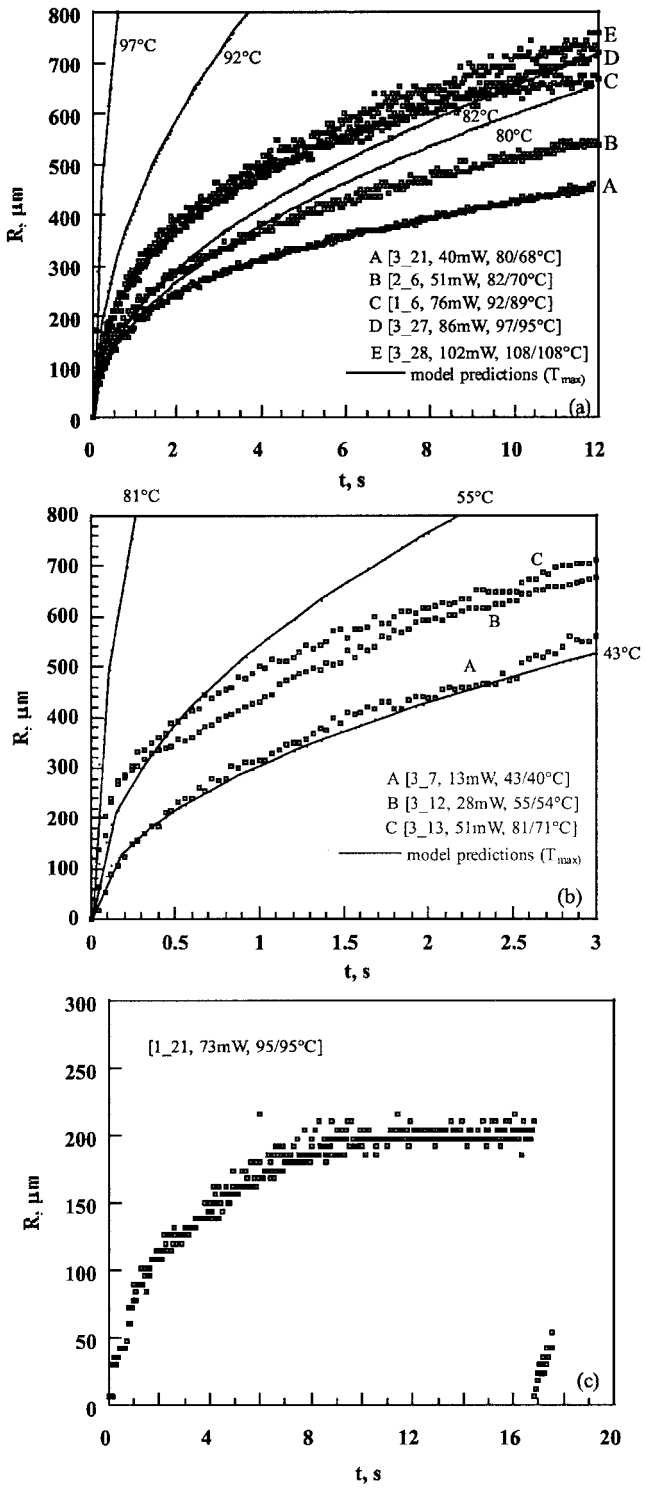

Figure 8. Single bubbles growing under different power and temperature of the heating thermistor.

(a) In water, (b) in *n*-heptane, (c) in glycerin/water solution. The model predictions for T_{max} of each run is also included for comparison.

radius is around 200 μm. Then, if the power is high enough, a new bubble arises at another spot on the thermistor, as shown in Figure 8c. More work is needed to elucidate this issue.

Regarding water and *n*-heptane, one may think that the progressive discrepancy between theoretical predictions for T_{max} and measured data is attributed to the temperature decay of the thermistor during bubble growth. To shed some light on this matter, Figure 9a and b provide contrast of a few growth curves obtained with water and heptane, respectively, against predictions drawn for both the T_{max} and T_{min} of each run. It is apparent that for both liquids the temperature decay of the heating thermistor might partially explain the discrepancy, but only in the lower power runs. On the contrary, for higher

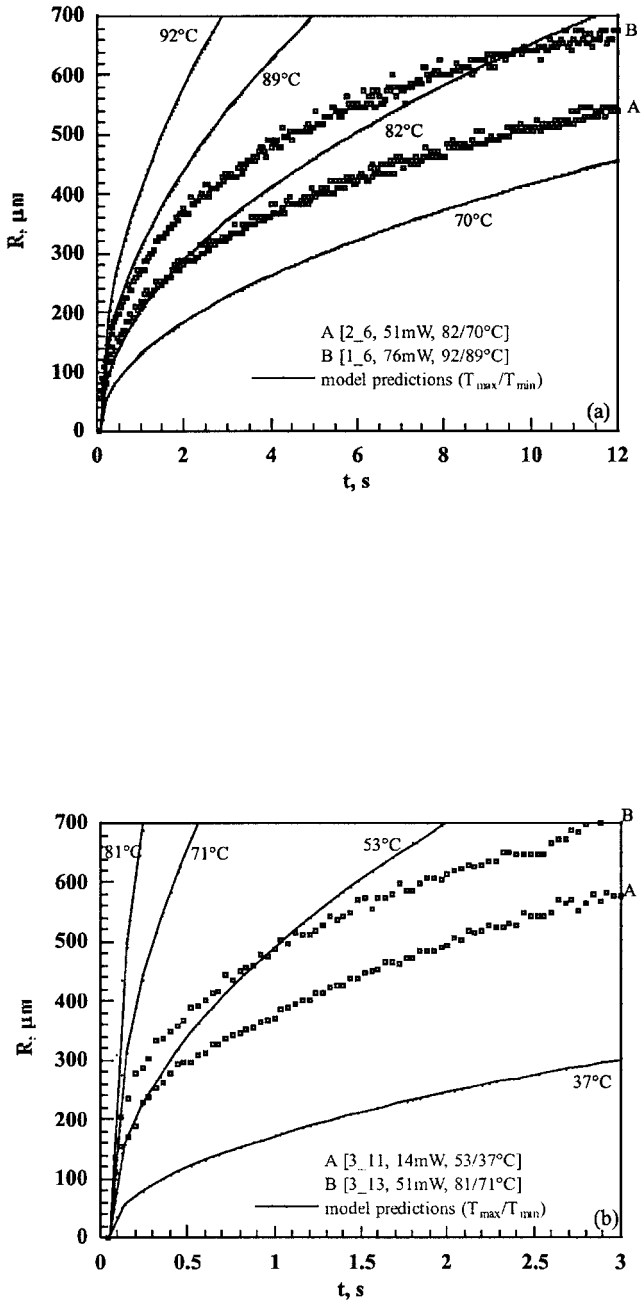

Figure 9. Comparison between measurements and theoretical predictions based on the observed T_{max} and T_{min} of each run.

(a) Water and (b) *n*-heptane.

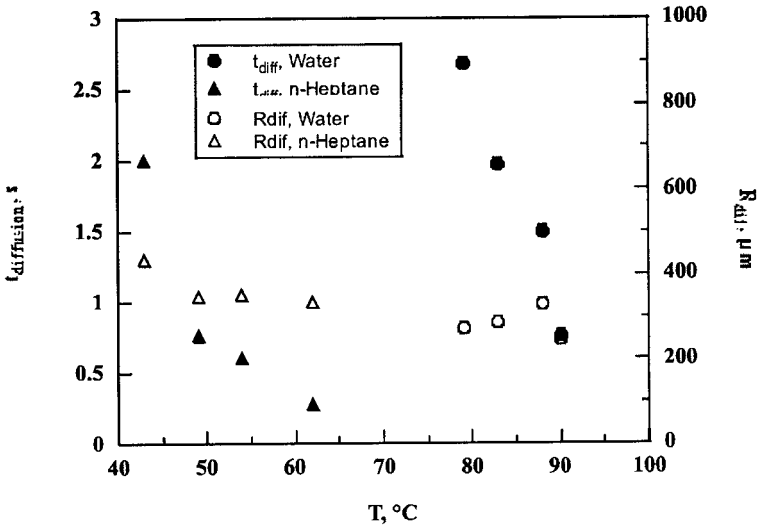

Figure 10. Isothermal effective diffusion time t_{dif} and isothermal effective diffusion radius R_{dif} vs. temperature.

powers the experimental growth rate is smaller even than the rate corresponding to T_{min}. Thus, an additional effect based on purely physical grounds must yet be sought.

Figure 10 examines the temperature dependency of the isothermal effective diffusion time t_{dif}, defined as the time for which the initial parabolic growth of our data is preserved within $\pm 3\%$ (the maximum overall experimental uncertainty). This parameter represents the *longest* fit of the data with the predictions of the isothermal model solved for a temperature (different but constant every time) selected between T_{max} and T_{min}. The bubble radius corresponding to this time is called (isothermal) effective diffusion radius R_{dif}, and is also displayed in Figure 10. Apparently, the present model is successful in describing the beginning of growth for a longer time in water than in heptane. Moreover, the goodness of the fit decreases with increasing temperature in both fluids. Taking into account the uncertainty in measurements, the effective diffusion radius may be considered virtually constant around 250–400 μm in all runs.

As mentioned earlier in the Theory section, assuming a constant bubble temperature in the self-similarity solution is equivalent to assuming that W, the heat input to the bubble, increases proportionally to $t^{1/2}$. A coarse way to check whether this condition is fulfilled is to calculate the experimental ratio of surface areas, $A_b/(A_{th} + A_b)$, and compare it with the ratio of powers, W/Q, where A_b is the experimentally measured surface area of the bubble, A_{th} is the surface area of the thermistor, and Q is the (constant) power delivered by the thermistor during a heat pulse. Such a comparison is presented in Figure 11 for *n*-heptane and for the run with the lowest power (13 mW) where the model predictions closely fit the data for most of the growth period (Figure 8b). The initial parabolic trend of the surface–area ratio with time is apparent, although on the whole there is a discrepancy with the corresponding power ratio. The discrepancy may only in part be attributed to the approximate geometrical calculation of surface areas, which assumed a perfectly spherical thermistor and also did not take into account the contact area between the bubble and the thermistor. A probable cause for the observed discrepancy is that the heat generated at the thermistor can be transformed to the liquid not only through the bubble but also directly (outside the bubble contact line).

In view of all the above, the disagreement between the self-similarity predictions and the experiments is probably attributable to the model assumption of an isolated bubble with a uniform temperature equal to that of the thermistor. It must also be noted at this point, that the main mechanism of energy consumption from the bubble to grow is the conduction of heat toward the liquid and not the latent heat requirements, as one may have intuitively expected. This result is easily deduced from a parametric analysis of Eqs. 23 to 25.

A tentative sequence of events during a heat pulse, which qualitatively reconciles most of the present experimental observations, is as follows: First, a thermal boundary layer develops rapidly around the thermistor (whether it reaches a steady state is not of concern). Shortly, a bubble emerges and grows inside this thermal boundary layer. One must recall here

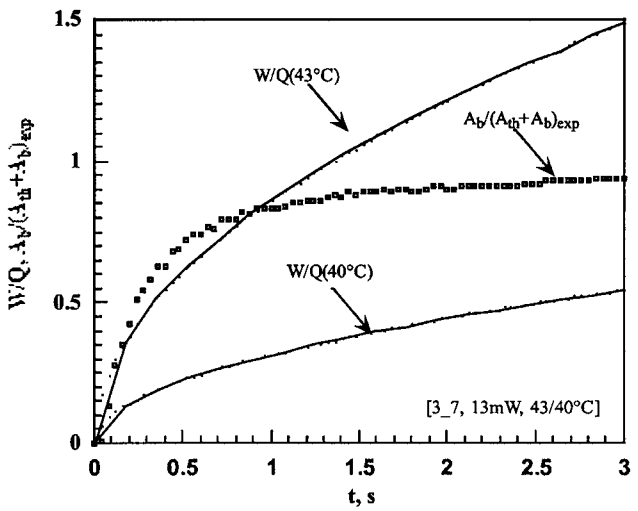

Figure 11. Comparison between the experimental ratio of surface areas $A_b/(A_{th} + A_b)_{exp}$ vs. the ratio of energies W/Q.

that in our experiments the growing bubble does not encapsulate the thermistor in its interior but extends at the side of the thermistor. As a result, the bubble during its growth is in contact with liquid layers of varying temperatures (along the thermal boundary layer around the thermistor) and has only a small contact with the thermistor itself. At the initial stages of growth, the bubble is small and is surrounded by quite warm liquid layers and therefore it is capable of keeping a constant temperature equal to that of the thermistor because the amount of energy needed by the bubble is small (heat conduction to the liquid is low). When the bubble exceeds a certain size (such as the critical radius 250–400 μm shown in Figure 10) it is exposed to considerably colder liquid layers and therefore requires a larger amount of power to maintain its temperature constant. This power is higher than the thermistor can provide so a temperature gradient develops inside the bubble with lower temperatures at its outer parts. Such a temperature gradient gives rise to Marangoni convection around the bubble surface, which also plays a role in drifting the bubble off the isothermal behavior. This may explain the reduced growth rates after a certain bubble size. Straub (1994) also argued about a similar temperature gradient inside the bubble in an effort to explain nucleate boiling in subcooled liquids.

For the case of high powers (and temperatures) of the thermistor, the bubble grows faster than the thermal boundary layer around the thermistor and so it is already from the beginning exposed to cold liquid. In such a case, conductive heat losses to the surrounding liquid dominate the growth process right from the start. This is a possible explanation for the drastic reduction in the amplification of growth rates beyond a certain thermistor temperature. Given that the key factor in this scenario is the rate of bubble growth, and not the temperature, this may also explain why the growth rates in heptane reach their maximum (limiting) value at a much lower temperature than in water.

Recalling information from the boiling studies reported in the literature, one might also be tempted to argue that, at relatively elevated temperatures, an evaporating microlayer comes gradually into play at the base of the bubble. This layer may serve as an additional barrier to heat transfer between the thermistor and the bubble. This idea was successfully used to explain the lower (than anticipated) growth rates of boiling bubbles (for example, Dhir, 1998; Plesset and Posperetti, 1977; Straub, 2000). However, it is doubtful whether an evaporating microlayer can effectively appear at temperatures below boiling.

To this end, although the mathematical model appears to capture the gross features of bubble growth, there are a few assumptions that must be relaxed to cope with all the details of the present experiments. The first calls for a bubble temperature that is not constant but its value is deduced from the solution of the energy equation for the given input power to the thermistor. The second deals with a temperature-dependent thermal conductivity and mass diffusivity. Finally, there are issues associated with the bubble being actually a segment of a sphere and the movement of its contact line, which require a 2-D analysis.

Conclusions

The bubble growth rates measured in *n*-heptane are much higher than those measured in water and glycerin/water solutions. This is so despite the fact that the heating powers (and heater temperatures) used in *n*-heptane are the lowest of all. Thus, the physical properties of the test fluid appear to dictate the rate of growth over and above the input power. For the same fluid, increasing the temperature of the heater produces a larger bubble, although this stops at a certain temperature beyond which any further increase has no significant effect on the size of the bubble.

A diffusion model is developed to describe the response of the system to local heat pulses. The simplified case of a bubble growing under constant temperature is solved to allow assessment of the contributing physical properties and experimental parameters.

In all fluids, bubbles grow fast at the beginning and gradually slow down at later stages. The first 1 or 2 s of growth are in agreement with the predictions of the diffusion model solved for the initial (maximum) temperature of the bubble. At later times these isothermal predictions fail to describe the data and the growth curve becomes approximately linear. Reliable measurements at these later stages of growth were made possible only because of the low-gravity conditions during the experiments, which allowed large and yet spherical bubbles to be recorded. The transition from the parabolic to the linear growth region indicates a departure from the isothermal growth mode, probably attributable to the steep temperature gradients that develop around the bubble. To the best of our knowledge this is the first time that such an observation was made.

Acknowledgments

We are thankful to ESA for kindly providing the parabolic flights. The support of Dr. Vladimir Pletser and Dr. Jorge Vago of ESA during the flights is gratefully acknowledged. We are particularly indebted to the many colleagues of the workshops in the Van der Waals–Zeeman Lab of the University of Amsterdam for their high-precision work in the design and construction of the flight apparatus.

Literature Cited

Arefmanesh, A., and S. G. Advani, "Diffusion-Induced Growth of a Gas Bubble in a Viscoelastic Fluid," *Rheol. Acta*, **30**, 274 (1991).

Arefmanesh, A., S. G. Advani, and E. E. Michaelides, "An Accurate Numerical Solution for Mass Diffusion Induced Bubble Growth in Viscous Liquids Containing Limited Dissolved Gas," *Int. J. Heat Mass Transfer*, **35**(7), 1711 (1992).

Barker, G. S., B. Jefferson, and S. J. Judd, "The Control of Bubble Size in Carbonated Beverages," *Chem. Eng. Sci.*, **57**, 565 (2002).

Birkhoff, G., R. S. Margulies, and W.A. Horning, "Spherical Bubble Growth," *Physics Fluids*, **1**(3), 201 (1958).

Bisperink, C. G. J., and A. Prins, "Bubble Growth in Carbonated Liquids," *Colloids Surf. A: Physicochem. Eng. Aspects*, **85**(2–3), 237 (1994).

Bontozoglou, V., and A. J. Karabelas, "Direct-Contact Steam Condensation with Simultaneous Noncondensable Gas Absorption," *AIChE J.*, **41**, 241 (1995).

Buehl, W. M., and J. W. Westwater, "Bubble Growth by Dissolution: Influence of Contact Angle," *AIChE J.*, **12**, 571 (1966).

Cable, M., and J. R. Frade, "The Influence of Surface Tension on the Diffusion-Controlled Growth or Dissolution of Spherical Bubbles," *Proc. R. Soc. Lond. A Phys. Sci.*, **420**, 247 (1988).

Campos, F. B., and P. L. C. Lage, "Heat and Mass Transfer Modeling during the Formation and Ascension of Superheated Bubbles," *Int. J. Heat Mass Transfer*, **43**, 2883 (2000).

Chen, T., and J. N. Chung, "Coalescence of Bubbles in Nucleate Boiling on Microheaters," *Int. J. Heat Mass Transfer*, **45**(11), 2329 (2002).

Clift, R., J. R. Grace, and M. E. Weber, *Bubbles, Drops and Particles*, Academic Press, New York (1978).

de Bruijn, R., R. J. J. van Diest, T. D. Karapantsios, A. C. Michels, W. A. Wakeham, and J. P. M. Trusler, "Heat Transfer in Pure Critical Fluids

Surrounded by Finitely Conducting Boundaries in Microgravity," *Physica A*, **242**, 119 (1997).
Dhir, V. K., "Boiling Heat Transfer," *Annu. Rev. Fluid Mech.*, **30**, 365 (1998).
Foster, P. P., A. H. Feiveson, R. Glowinski, M. Izygon, and A. M. Boriek, "A Model for Influence of Exercise on Formation and Growth of Tissue Bubbles during Altitude Decompression," *Am. J. Physiol. Regul. Integr. Comp. Physiol.*, **279**(6), R2304 (2000).
Glas, J. P., and J. W. Westwater, "Measurements of the Growth of Electrolytic Bubbles," *Int. J. Heat Mass Transfer*, **7**, 1427 (1964).
http://factrio.jst.go.jp/cgi-bin/al_m_login.csh
Jones, F., G. M. Evans, and K. P. Galvin, "The Cycle of Bubble Production from a Gas Cavity in a Supersaturated Solution," *Adv. Colloid Interface Sci.*, **80**(1), 51 (1999a).
Jones, F., G. M. Evans, and K. P. Galvin, "Bubble Nucleation from Gas Cavities—A Review," *Adv. Colloid Interface Sci.*, **80**(1), 27 (1999b).
Kislyakov, Yu. Ya., and A. V. Kopyltsov, "The Rate of Gas-Bubble Growth in Tissue under Decompression. Mathematical Modeling," *Respir. Physiol.*, **71**(3), 299 (1988).
Lee, H. S., and H. Merte, Jr., "Spherical Vapor Bubble Growth in Uniformly Superheated Liquids," *Int. J. Heat Mass Transfer*, **39**(12), 2427 (1996a).
Lee, H. S., and H. Merte, Jr., "Hemispherical Vapor Bubble Growth in Microgravity: Experiments and Model," *Int. J. Heat Mass Transfer*, **39**(12), 2449 (1996b).
Lide, D. R., and H. P. R. Frederikse, *CRC Handbook of Chemistry and Physics*, 77th Edition, CRC Press: Boca Raton, FL (1996–1997).
Mikic, B. B., W. M. Rohsenow, and P. Griffith, "On Bubble Growth Rates," *Int. J. Heat Mass Transfer*, **13**, 657 (1970).
Payvar, P., "Mass Transfer Controlled Bubble Growth during Rapid Decompression of a Fluid," *Int. J. Heat Mass Transfer*, **30**(4), 699 (1987).
Perry, R. H., and C. H. Chilton, *Chemical Engineer's Handbook*, 5th International Student Edition, McGraw-Hill/Kogakusha, New York/Tokyo, Japan (1973).
Picker, G, and J. Straub, "Interfacial Mass Transfer Studies on Vapor Bubbles in Microgravity," Proc. of United Engineering Foundation Conf., Sept. 1999, V. K. Dhir, ed., Kahuku, Oahu, Hawaii, pp. 72–79 (2000).
Plesset, M. S., and A. Prosperetti, "Flow of Vapor in Liquid Enclosure," *J. Fluid Mech.*, **78**(3), 433 (1977).
Plesset, M. S., and S. S. Sadhal, "On the Stability of Gas Bubbles in Liquid–Gas Solutions," *App. Sci. Res.*, **38**, 133 (1982).
Plesset, M. S., and S. A. Zwick, "The Growth of Vapor Bubbles in Superheated Liquids," *J. Appl. Phys.*, **25**, 493 (1954).
Reid, R. C., J. M. Prausnitz, and B. E. Poling, *The Properties of Gases and Liquids*, 4th Edition, McGraw-Hill, New York (1986).
Robinson, A. J., and R. L. Judd, "Bubble Growth in a Uniform and Spatially Distributed Temperature Field," *Int. J. Heat Mass Transfer*, **44**, 2699 (2001).
Rosner, D. E., and M. Epstein, "Effects of Interface Kinetics, Capillarity and Solute Diffusion on Bubble Growth Rates in Highly Supersaturated Liquids," *Chem. Eng. Sci.*, **27**, 69 (1972).
Saddy, M., and G. J. Jameson, "Experiments on the Dynamics of Phase Growth," *Chem. Eng. Sci.*, **26**(5), 675 (1971).
Scriven, L. E., "On the Dynamics of Phase Growth," *Chem. Eng. Sci.*, **10**, 1 (1959).
Shaw, B. D., and M. L. Pantoya, "Growth and Application of Large Spherical Bubbles Using Reactive Gases," *Int. Commun. Heat Mass Transfer*, **27**(6), 807 (2000).
Srinivasan, R. S., W. A. Gerth, and M. R. Powell, "A Mathematical Model of Diffusion Limited Gas Bubble Dynamics in Tissue with Varying Diffusion Region Thickness," *Respir. Physiol.*, **123**, 153 (2000).
Straub, J., "The Role of Surface Tension for Two-Phase Heat and Mass Transfer in the Absence of Gravity," *Exp. Thermal Fluid Sci.*, **9**, 253 (1994).
Straub, J., "Boiling Heat Transfer and Bubble Dynamics in Microgravity," *Adv. Heat Transfer*, **35**, 57 (2000).
Straub, J., M. Zell, and B. Vogel, "Pool Boiling in a Reduced Gravity Field," Proc. of the 9th Int. Heat Transfer Conf., G. Hetserony, ed., Hemisphere, New York, pp. 129–155 (1990).
Straub, J., M. Zell, and B. Vogel, "Boiling under Microgravity Conditions," Int. Proc. First European Symposium Fluids in Space, Ajaccio, France, 1991, ESA SP-353 (1992).
Strenge, P. H., A. Orell, and J. W. Westwater, "Microscopic Study of Bubble Growth during Nucleate Boiling," *AIChE J.*, **7**, 578 (1961).
Van Liew, H. D., and M. E. Burkard, "Simulation of Gas Bubbles in Hypobaric Decompressions: Roles of O_2, CO_2, and H_2O," *Aviation Space Environ. Med.*, **66**(1), 50 (1995).
Vrentas, J. S., C. M. Vrentas, and H. C. Ling, "Equations for Predicting Growth or Dissolution Rates of Spherical Particles," *Chem. Eng. Sci.*, **38**, 1927 (1983).
Yoo, H. J., and C. D. Han, "Oscillatory Behavior of a Gas Bubble Growing (or Collapsing) in Viscoelastic Liquids," *AIChE J.*, **28**(6), 1002 (1982).

Appendix

To obtain numerical results, the integral in Eq. 22b is transformed to the following more convenient form

$$\varphi(z) = 2z^2 \int_0^1 \exp\{-z^2[(1-y)^{-2} - 2y - 1]\}dy \quad \text{(A1)}$$

The above is integrated numerically by transforming it to an ordinary differential equation and using an integrator with self-adjustable step and prespecified accuracy.

Instead of numerically computing the integral (Eq. A1), the following correlation can be used with local accuracy much better than 1%

$$\varphi(z) = \sqrt{\pi/3}\,(z - 4/9) \qquad \text{for } z > 6 \quad \text{(A2)}$$

$$\varphi(z) = 1.0022z - 0.3232 \qquad \text{for } 6 > z > 1.22 \quad \text{(A3)}$$

$$\varphi(z) = (2 - 3.3745z + 4.1675z^2 - 2.9305z^3 + 0.834z^4)z^2 \qquad \text{for } z < 1.22 \quad \text{(A4)}$$

$$\varphi(z) = \Psi \Rightarrow z = (0.7063 + 0.4545\sqrt{\Psi} + 0.1591\Psi)\sqrt{\Psi} \qquad \text{for } \Psi < 0.89 \quad \text{(A5)}$$

$$z = \frac{\Psi + 0.3232}{1.0022} \qquad \text{for } 5.7 > \Psi > 0.89 \quad \text{(A6)}$$

$$z = \frac{\Psi}{\sqrt{\pi/3}} + 4/9 \qquad \text{for } \Psi > 5.7 \quad \text{(A7)}$$

Manuscript received Feb. 17, 2003, and revision received Jan. 14, 2004.